

Observing microscopic structures of a relativistic object using a time-stretch strategy

E. Roussel^{1,2}, C. Evain^{1,2}, M. Le Parquier², C. Szwej^{1,2}, L. Manceron³, J.-B. Brubach³, M.-A. Tordeux³, J.-P. Ricaud³, L. Cassinari³, M. Labat³, M.-E. Couprie³, P. Roy³, S. Bielawski^{1,2}

(1) *Laboratoire PhLAM, UMR CNRS 8523, Université Lille 1, Sciences et Technologies, 59655 Villeneuve d'Ascq, France*

(2) *Centre d'Étude Recherches et Applications (CERLA), 59655 Villeneuve d'Ascq, France*

(3) *Synchrotron SOLEIL, L'Orme des Merisiers, Saint-Aubin, BP 48, 91192 Gif-sur-Yvette Cedex, France*

(Dated: December 7, 2024)

PACS numbers: 41.60.Ap, 29.27.Bd, 05.45.-a

Emission of light by a single electron moving on a curved trajectory (synchrotron radiation) is one of the most well-known fundamental radiation phenomena. However experimental situations are more complex as they involve many electrons, each being exposed to the radiation of its neighbors. This interaction has dramatic consequences, one of the most spectacular being the spontaneous formation of spatial structures inside electron bunches. This fundamental effect is actively studied as it represents one of the most fundamental limitations in electron accelerators, and is suspected to be at the origin of strong electromagnetic emissions in solar flares. Here we demonstrate the possibility to directly observe electron microstructures with subpicosecond resolution in a storage ring accelerator. The needed resolution is obtained using a novel time-stretch strategy, consisting in slowing-down the phenomena before recording. This opens the way to unprecedented possibilities for analyzing and mastering new generation high power coherent synchrotron sources.

Interaction of a relativistic electron bunch with its own created electromagnetic field can lead to the so-called *microbunching instability*. It is encountered in systems based on linear accelerators [1], the Sun [2–4], as well as in the widely-used storage rings facilities [5–14] (synchrotron radiation facilities), where electron bunches are forced to circulate onto a closed loop trajectory. Above a threshold electron bunch density, a longitudinal modulation or *pattern* appears with a characteristic period at the millimeter or sub-millimeter scale [5–7, 15]. This structure emits intense pulses of terahertz radiation (typically more than 100000 times normal synchrotron radiation), called Coherent Synchrotron Radiation (CSR). Each CSR pulse shape may be viewed as an “image” of the electron bunch microstructure.

As a consequence, a particularly efficient way to study this fundamental physical effect consists in using existing *user-oriented* storage rings (i.e., synchrotron radiation facilities). Indeed, recording CSR pulses emitted at each turn in such a storage ring would be theoretically

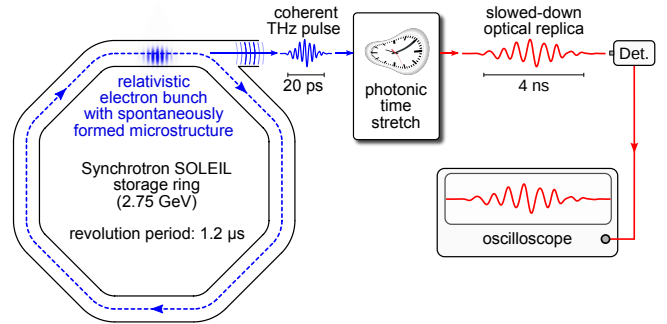


FIG. 1: General principle of the experiment. A relativistic electron bunch circulating in the SOLEIL storage ring (2.75 GeV) presents microstructures, that evolve in a complex way. The coherent THz radiation emitted at a bending magnet carries the information on the microstructure shape, but is too fast (at picosecond scale) to be recorded by traditional means. The present strategy consists in “slowing-down” the information in order to obtain an optical replica at the nanosecond scale, so that a conventional oscilloscope can be used for the recording.

sufficient to follow the electron microstructure evolution over a long time. This has been recently demonstrated in a special case where the microstructure wavelength is in the centimeter range and CSR emission occurs in the tens of GHz range [16], thus being accessible to conventional electronics. However, in most storage rings such as ALS [6], ANKA [10], BESSY [7], DIAMOND [11, 12], ELETTRA [11], or SOLEIL [14], etc., the CSR emission occurs at frequencies that are so high (above 300 GHz for the present case of SOLEIL) that no suitable recording electronics is available at the moment, nor expected in the near future.

Here, we propose a strategy that overcomes these limitations, and thus enables such fundamental studies in many storage ring facilities. It consists in “slowing down” the signals so that they can be recorded by conventional oscilloscopes (Fig. 1). This is a two-step process as shown in Figure 2. First, the THz CSR pulse is encoded into a laser pulse, using the well established technique of THz electro-optic sampling [10, 17–19]. Then the key point is to use a setup based on the so-called *photonic time-*

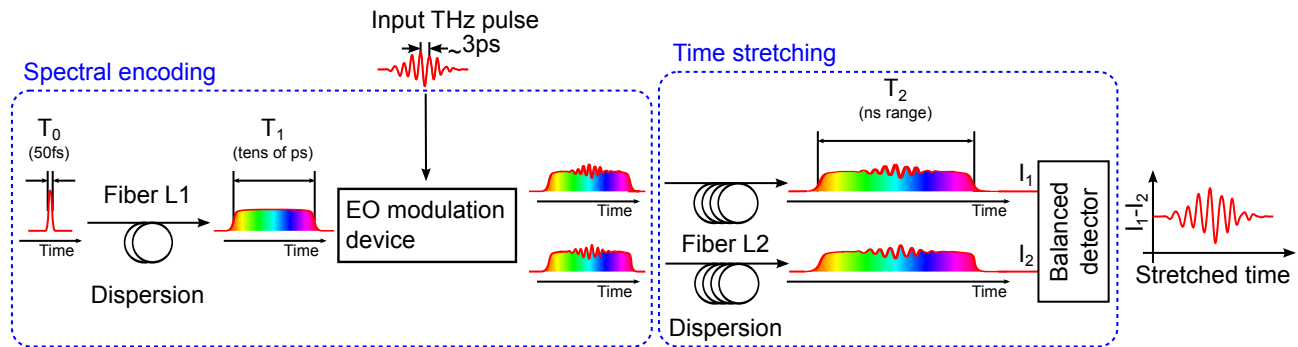


FIG. 2: Principle of the photonic time-stretch device realized for slowing down the information, while keeping a high sensitivity. The THz pulse under investigation is first encoded into a chirped laser pulse, using an electro-optic crystal (“EO modulation device”). This device (see Fig. 6 for details) provides two complementary outputs. Then the optical information of each output is simply stretched from picoseconds to nanoseconds by propagation in a long fiber (2 km). Balanced detection is performed between the two stretched laser pulses, thus providing a very high sensitivity for the device by removing the “DC” background. Details of the optical system are presented in the Methods section.

stretch strategy [20–22], which consists in dispersing the pulses in a long fiber. Under some condition on the fiber length L_1 , the output pulse is a replica of the original signal, except that is slowed down by a magnification factor (or stretch factor) [23]:

$$M = 1 + \frac{L_2}{L_1}, \quad (1)$$

where L_1 and L_2 are the input and output fiber lengths ($L_1 = 10.7$ m and $L_2 = 2$ km for the results presented hereafter, leading to a stretch factor $M = 190$). Using such a strategy instead of the classical *spectral encoding* [17–19] method presents two advantages: (i) a much higher acquisition rate (i.e., the number of recorded terahertz pulses per second), which is directly linked to the laser repetition rate, and (ii) the possibility of performing balanced detection [24], a crucial point for reaching high sensitivity.

The time-stretch THz recording system (detailed in Figure 6) was able to acquire 88×10^6 terahertz pulses per second, and its sensitivity was measured to be 37 V/cm inside the crystal (see Methods). This allowed us to record the terahertz CSR pulses (electric field, including envelope and carrier) emitted at each turn (i.e., every $1.2 \mu\text{s}$) at the AILES beamline of the SOLEIL storage ring.

First experiments with the time-stretch acquisition setup allowed us to record the THz CSR for each revolution in the ring, and to visualize the predicted microstructure in the electron bunch circulating at Synchrotron SOLEIL. The structure is clearly visible in Figure 3, which represents a typical series of individual pulses, recorded at successive round-trips.

Furthermore, the new type data thus obtained contain extremely detailed information on the long-term evolution of the structures. In order to summarize the dynamical features, we displayed the pulse evolution of Fig. 3 as a colormap versus the longitudinal coordinate, and the number of turns in the storage ring (Fig. 4). It clearly

appears that –though their evolutions are very complex– the structures are constituted of oscillations with a characteristic wavenumber in the millimeter range (more precisely 10 cm^{-1} , or 0.3 THz as shown in the inset of Fig. 3). This is consistent with previous indirect observations, by spectrometric measurements, of a strong terahertz emission peak at 10 cm^{-1} [14]. Moreover, the recordings (as in Fig. 4) systematically revealed complex drifting evolution during the revolutions, that remind the ubiquitous irregular behaviors that occur in fluid dynamics [25]. We believe that this new detailed data will provide a real platform for testing and refining theoretical models of relativistic electron bunch dynamics.

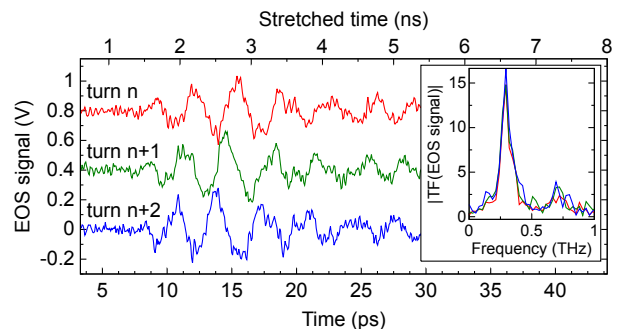


FIG. 3: Typical single-shot recordings of coherent THz pulses, which carry the information on the electron microstructure. The lower scale corresponds to the real time of the phenomenon. The upper scale corresponds to the time at the oscilloscope input (i.e., after the photonic time stretch by a factor 190). The time between pulses is of the order of $1 \mu\text{s}$, but the system is actually recording one signal every 12 ns. The effective A/D conversion speed is 15 Tera samples/s. Inset: Power Fourier spectra of the three pulses.

Several important features of the experimental observations can be reproduced with already existing theoretical models [5, 14, 26, 27], where only longitudinal dynamics of the electrons is taken into account. Each electron

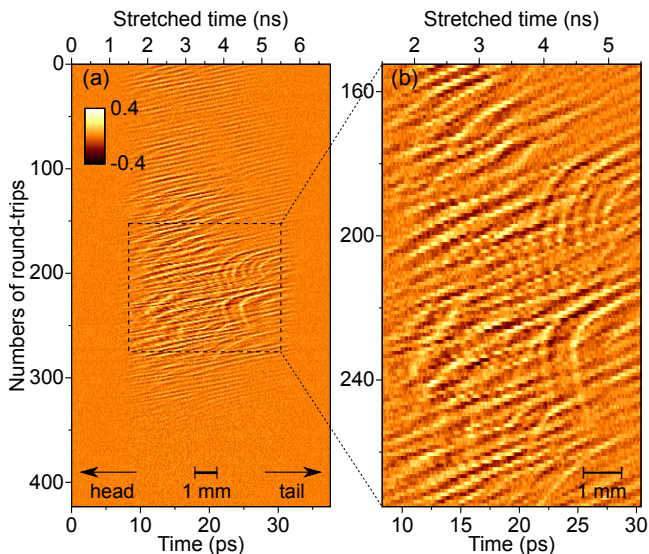


FIG. 4: Recorded CSR pulses (i.e., containing the information on the electron bunch longitudinal modulation) versus the number of round-trips in the storage ring. (b) is a zoom on the rectangle part in (a).

i is characterized by its instantaneous position z_i and energy variable δ_i . A map (at each turn n) can then be written for the evolutions of z_i^n and δ_i^n . Taking the continuous limit for the number of round-trips n [28, 29]:

$$\frac{dz_i}{dt} = -\eta c \delta_i \quad (2)$$

$$\frac{d\delta_i}{dt} = -\left(\frac{\omega_s^2}{\eta c}\right) z_i - \left(\frac{2}{\tau_s}\right) \delta_i - F(z_i) - \eta_N \xi(t), \quad (3)$$

where t is a continuous time associated to the number of round-trips n . $\delta_i(t) = [E_i(t) - E_R]/E_R$, with $E_i(t)$ the electron energy, and E_R the reference energy corresponding to the synchronous electron (2.75 GeV here). $F(z_i)$ characterizes the electric field at position z_i created by the whole electron bunch, and is the main ingredient of the instability. We use here the same form as in previous studies of SOLEIL [14]. $\omega_s/2\pi$ is the synchrotron frequency (not to be confused with the storage ring revolution time), and τ_s is the synchrotron damping time. c is the speed of light in vacuum and η measures the dependence of the round-trip time with the electron energy. $\eta_N \xi$ is a gaussian white noise term, with $\langle \xi(t)\xi(t') \rangle = \delta(t - t')$. Parameter values are given in the Methods section.

Typical numerical results are presented in Fig. 5. When the electron bunch charge exceeds a threshold, finger-like structures are spontaneously formed in the electrons phase space (Fig. 5a). Furthermore, the whole electron bunch distribution experiences a global rotation near the so-called synchrotron frequency (4.64 kHz here), and evolves in a bursting and irregular way.

The longitudinal electron bunch shape (Fig. 5b) is deduced from the vertical projection of the phase space

distribution (Fig. 5a). Then the CSR THz field at the electron bunch location (Fig. 5c) is deduced from the electron bunch shape (Fig. 5b). As can be seen in Fig. 5c, only the fast variations lead to a significant coherent terahertz field. This natural “AC-coupling” is an advantage for the observation as it removes the global (slow) electron bunch shape, and let pass only the important information. Because the electron bunch distribution rotates counter-clockwise in phase-space (see Fig. 5a and supplementary movie), the microstructures drift along the longitudinal position toward the head of the electron bunch (Fig. 5c). The drift of the structures (in Figs. 4 and 5d) can thus be interpreted as a consequence of the formation of “fingers” in the lower part of phase space (Figs. 5a). Main features of the theoretical predictions are found in relatively satisfying agreement with the new experimental findings.

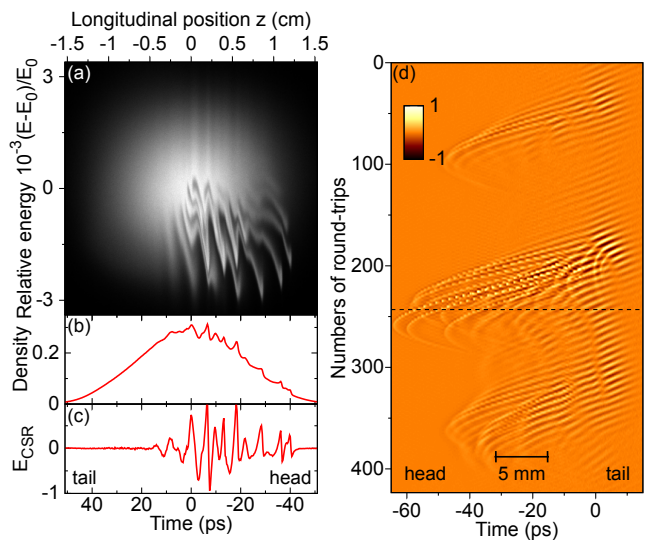


FIG. 5: Numerical simulation of the relativistic electron bunch dynamics. (a) Distribution of the electrons in position-energy phase space (1.1×10^8 particles are taken into account in the simulation). The pattern globally rotates at a slow frequency near 4.64 kHz, and evolves in a complex way (see supplementary movie). (b) Electron bunch profile (i.e., the projection of (a) onto the z axis), and (c) CSR field. (d) evolution of the CSR pulse shapes versus number of round-trips. The dashed line corresponds to the (c) pulse.

In conclusion, the present time-stretch strategy allows one to perform a “time-lapse observation” of microscopic structures that appear within charged relativistic objects. The advantages over classic single-shot electro-optic sampling strategies are a simultaneous improvement on both the acquisition rate and the sensitivity. Such quantitative studies open-up to a new level of understanding of electron beam dynamics, and severe tests of theoretical models. We believe that this strategy may be a key contribution in situations where high acquisition rate measurements are needed. Straightforward applications concern the investigation of the THz pulses emit-

ted by other storage rings, and by terahertz free-electron lasers. The technique can also be transferred to high-repetition rate linear accelerators, provided an electro-optic sampling system can be used [18]. Perspectives in ultrafast spectroscopy are also envisaged, as the instantaneous THz spectrum can be straightforwardly deduced from the electric field shape (inset of Fig. 3). In addition to the THz domain, the present time-stretch strategy also opens new possibilities at short wavelengths. Important perspectives to be explored concern the monitoring of optical pulses from high-repetition rate EUV and X-ray Free-Electron Lasers, for instance by associating the time-stretch strategy to transient reflectivity setups [30, 31].

Methods

A. Ultrafast recording setup

The detailed setup is presented in Fig. 6. It exclusively uses off-the-shelf components, and is composed of three parts:

- A classical system for generation of chirped laser pulses, using a femtosecond laser and a dispersive fiber.
- A classical electro-optic modulation system, based on the Pockels effect in a GaP crystal.
- A specially designed balanced time-stretch device. This setup disperses the optical pulses up to the nanosecond range. Thus we can achieve simultaneously a high repetition rate, and at the same time a high sensitivity thanks to the possibility of the balanced detection. This is the key point of the setup.

1. Production of the stretched laser pulses

We use a femtosecond Ytterbium-doped fiber laser (Orange) from MENLO GmbH. The emitted pulses have a spectral bandwidth of 50 nm, and the total output average power is 40 mW. The repetition rate is chosen at 88 MHz, which corresponds to $1/4$ *th* of the RF frequency of Synchrotron SOLEIL and 104 times the electron revolution frequency. It is synchronized on the RF clock of the storage ring using a RRE-Synchro system from MENLO GmbH.

The pulses are chirped by a polarization-maintaining fiber (PM 980), which length determines the temporal window of the acquisition (typically few tens of picoseconds). The length L_1 which is used in the calculation of the stretch factor $M = 1 + L_2/L_1$ is the sum of two components: the actual length of the fiber used after the laser (10 m here), and a small contribution due to pulse

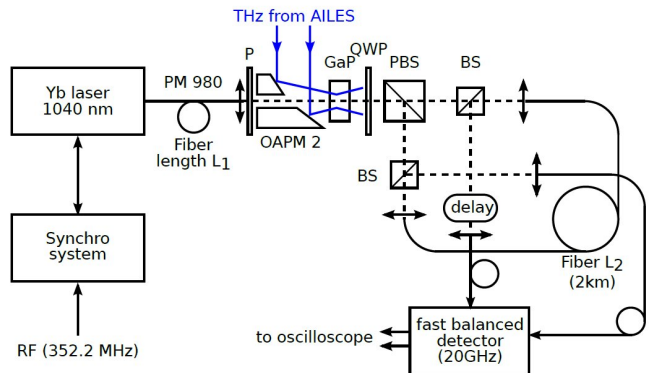


FIG. 6: Experimental setup for recording the THz pulses at 88 MHz acquisition rate. P: polarizer, OAPM: off-axis (gold-coated) parabolic mirror. GaP: Gallium Phosphide crystal. QWP: achromatic quarter-wave plate. PBS: polarizing beam-splitter. BS: beam-splitter with low polarization-dependent losses. The 2 km fiber is an HI1060 from Corning. All fiber collimating and focusing lenses have 11 mm focal length. (Delay) is a delay line, allowing to adjust the relative delay between the two balanced detector inputs.

dispersion inside the laser (estimated to 0.7 m of propagation in a PM980 fiber). Thus we took $L_1 = 10.7$ m, leading to $M \approx 190$.

A polarizer is placed at the output in order to remove possible spurious components with the wrong polarization.

2. Electro-optic modulation device

This part corresponds to the *EO modulation device* in Fig. 2, and from (P) to (PBS) in Fig. 6. The THz radiation available at the focusing point of the beamline is first collimated using an off-axis parabolic mirror (not shown in Fig. 6), with 101.6 mm focal length. It is then focused in the GaP crystal using an off-axis gold-coated parabolic mirror (OAPM2 in S) with 50.8 mm focal length, and a 3 mm hole. The laser and the THz radiation interact in a [110]-cut GaP crystal with 5 mm length ($10 \times 10 \times 5$ mm³). The [-110] axis is parallel to the polarizations of the laser and the THz beam. An achromatic quarter-wave plate is inserted after the GaP crystal. Its optical axis oriented at $\pi/4$ with respect to the laser polarization. Finally, a polarizing cube beam-splitter (PBS) provides the two outputs of the EO modulation device. At the outputs of the PBS, the pulses contain an intensity modulation which is a “replica” of the THz pulses, and the two outputs are modulated in opposite phase.

3. Time-stretching of the two optical pulses, using a single fiber

Instead of using physically different fibers for the final dispersion (Fig. 2), we use a variant that is much more robust from the experimental point of view. As can be seen in Fig. 6, the two output pulses of the polarizing cube beam-splitter are sent in the same fiber, in opposite directions. Finally, two beam-splitters extract the two pulses, which are sent to a fast balanced photoreceiver. This technique (which reminds the idea of the Sagnac loop) permits to obtain the same path on the two laser pulses even when the fiber optical length fluctuates.

The L_2 fiber is an HI1060 from Corning with 2 km length (and an overall attenuation of the order of 3 dB), and the beam-splitters (BS) are chosen to have low polarization-dependent losses (Newport 05BC17MB.2). This choice for L_2 leads to stretched pulses of ≈ 4.5 ns, and 1.35 mW peak power is typically detected in each balanced photoreceiver channel input.

B. Recording electronics

The detection and subtraction between the two stretched signals is performed using a DSC-R412 InGaAs amplified balanced photodetector from Discovery Semiconductors, with 20 GHz bandwidth and 2800 V/W gain (specified at 1500 nm). The two differential outputs of the detector are sent on a Lecroy LabMaster 10i oscilloscope with 36 GHz bandwidth, 80 GS/s sample rate on each channel, and a memory of 256 Mega samples.

1. Data processing

In absence of THz signal, the recorded balanced signal presents a non-zero shape which corresponds to imperfections of the setup, in particular small polarization dependent losses (that depend on wavelength). Since this “background” signal is deterministic (i.e., is the same for each laser pulse), it is easily removed from the signal, by a simple subtraction.

2. Transport of the terahertz beam

We operated the time-stretch setup at the A branch of the AILES beamline, just before the interferometer (see Ref. [32] for the beamline detail). The focusing point was imaged onto the GaP crystal, using a telescope composed of a 101.6 mm focal length off-axis parabolic mirror (not shown in Fig. 6) and a 50.8 mm off-axis parabolic mirror (OAPM2 in Fig. 6).

C. Performances of the setup

The special setup presented in Fig. 6 provides higher acquisition rates (in terms of number of pulses per second) than classical spectral encoding methods. The reason is that oscilloscopes can nowadays reach much higher data acquisition rates (80 Giga samples/s here) than the cameras which are necessary for spectral encoding. Here, the acquisition rate capability is limited by the repetition rate of the laser, namely 88 MHz.

At the same time, the setup allows us to perform acquisition with higher sensitivity than the traditional single-shot electro-optic sampling, because, of the possibility to achieve balanced detection at the analog level. The sensitivity is here mainly limited by the noise of the amplified balanced detector. The RMS noise on the finally recorded signal can be easily measured, and this gives a measure of the system sensitivity. The RMS noise (over the 20 GHz bandwidth of the photodetector) corresponds to a birefringence-induced phase shift in the GaP of 3.2×10^{-3} Radian. Assuming that the relevant electro-optic coefficient of GaP is $r_{41} = 0.97$ pm/V, and neglecting the THz frequency dependence of r_{41} , the sensitivity is estimated to be 37 V/cm (inside the crystal) near the laser pulse peak.

The SOLEIL storage ring was operated in single bunch, normal alpha mode, with natural bunch length $\sigma_z = 4.59$ mm, relative energy spread $\sigma_\delta = 1.017 \times 10^{-3}$, and a momentum compaction factor $\alpha = 4.38 \times 10^{-4}$. The ring was operated at a current of 15 mA, which is above the microbunching instability threshold (≈ 10 mA). Other parameters are described in Ref. [14]. The model parameters η and η_N are defined by $\alpha - \frac{1}{\gamma^2}$ and $\eta_N = \frac{du_z}{T_0}$, with T_0 the storage ring revolution time.

I. ACKNOWLEDGEMENTS

The work was supported by the Agence Nationale de la Recherche (projet Blanc DYNACO 2010-042301), the Université Lille 1 (BQR 2012) and used HPC resources from GENCI TGCC/IDRIS (2013-x2013057057, 2014x2014057057). The CERLA is supported by the French Ministère chargé de la Recherche, the Région Nord-Pas de Calais and FEDER.

Contributions

The acquisition system was designed, realized and operated by CS, ER, CE, MLP, SB, data analysis by CE and CS. Special operation of the AILES beamline was performed by LM, JBB, and PR (also project manager on SOLEIL side). Accelerator conditions were managed by MAT, diagnostics by ML, laser synchronization electronics by JPR, LC, MEC. MEC also participated to the early stages of the project elaboration. Numerical simu-

lations were performed by ER, simulation code development by ER and SB.

-
- [1] Venturini, M. Microbunching instability in single-pass systems using a direct two-dimensional vlasov solver. *Phys. Rev. ST Accel. Beams* **10**, 104401 (2007).
- [2] Kaufmann, P. & Raulin, J.-P. Can microbunch instability on solar flare accelerated electron beams account for bright broadband coherent synchrotron microwaves? *Physics of plasmas* **13**, 070701 (2006).
- [3] Kaufmann, P. & Raulin, J.-P. Sub-terahertz, microwaves and high energy emissions during the 6 december 2006 flare, at 18:40 ut. *Physics of plasmas* **255**, 131 (2009).
- [4] Klopff, J. M., Kaufmann, P., Raulin, J.-P., & Szpigiel, S. The contribution of the microbunching instability to solar flare emission in the ghz to thz range of frequencies. *The astrophysical journal* **791**, 31 (2014).
- [5] Stupakov, G. & Heifets, S. Beam instability and microbunching due to coherent synchrotron radiation. *Phys. Rev. ST Accel. Beams* **5**, 054402 (2002).
- [6] Byrd, J. M. *et al.* Observation of broadband self-amplified spontaneous coherent terahertz synchrotron radiation in a storage ring. *Phys. Rev. Lett.* **89**, 224801 (2002).
- [7] Abo-Bakr, M., Feikes, J., Holldack, K., Wüstefeld, G. & Hübers, H.-W. Steady-state far-infrared coherent synchrotron radiation detected at bessy II. *Phys. Rev. Lett.* **88**, 254801 (2002).
- [8] Hashimoto, S., Shoji, Y., Ando, A. & Takahashi, T. Observation of coherent synchrotron radiation at newsbaru. In *Proceedings of the 2005 Particle Accelerator Conference, Knoxville, Tennessee*, 4188–4190 (2005).
- [9] Mochihashi, A., Hosaka, M., Katoh, M., Shimada, M. & Kimura, S. Observation of THz synchrotron radiation bursts in UVSOR-II storage ring. In *Proceedings of the 2006 European Particle Accelerator Conference, Edinburgh, Scotland*, 3380 (2006).
- [10] Judin, V. *et al.* Spectral and temporal observations of csr at anka. In *Proceedings of the 2012 IPAC conference, New Orleans, Louisiana (USA)*, 4761 (2012).
- [11] Martin, I., Thomas, C., Bartolini, R. & Adams, J. Modelling the steady-state csr emission in low-alpha mode at the diamond storage ring. In *Proceedings of the 2012 International Particle Accelerator Conference, New Orleans, USA*, 1677 (2012).
- [12] Wüstefeld, G. *et al.* Coherent thz measurements at the metrology light source. In *Proceedings of the 2010 International Particle Accelerator Conference, Kyoto, Japan* (2010).
- [13] Karantzoulis, E., Penco, G., Perucchi, A. & Lupi, S. Characterization of coherent THz radiation bursting regime at ELETTRA. *Infrared Physics and Technology* **53**, 300 (2010).
- [14] Evain, C. *et al.* Spatio-temporal dynamics of relativistic electron bunches during the micro-bunching instability in storage rings. *EPL* **98**, 40006 (2012).
- [15] Warnock, R. L. Study of bunch instabilities by the nonlinear Vlasov-Fokker-Planck equation. *Nucl. Instrum. Meth. Phys. Res., Sect. A* **561**, 186–194 (2006).
- [16] Roussel, E. *et al.* Microbunching instability in relativistic electron bunches: Direct observations of the microstructures using ultrafast YBCO detectors. *Phys. Rev. Lett.* **113**, 094801 (2014).
- [17] Jiang, Z. & Zhang, X.-C. Electro-optic measurement of thz field pulses with a chirped optical beam. *Appl. Phys. Letters* 1945 (1998).
- [18] Wilke, I. *et al.* Single-shot electron-beam bunch length measurements. *Phys. Rev. Lett.* **88**, 124801 (2002). URL <http://link.aps.org/doi/10.1103/PhysRevLett.88.124801>.
- [19] Müller, F. *et al.* Electro-optical measurement of sub-ps structures in low charge electron bunches. *Phys. Rev. ST Accel. Beams* **15**, 070701 (2012). URL <http://link.aps.org/doi/10.1103/PhysRevSTAB.15.070701>.
- [20] Coppinger, F., Bhushan, A. & Jalali, B. Photonic time stretch and its application to analog-to-digital conversion. *IEEE Trans. on Microwave Theory and Techniques* **47**, 1309 (1999).
- [21] Honeycutt, R. L. Stochastic runge-kutta algorithms. i. white noise. *Phys. Rev. A* **45**, 600–603 (1992). URL <http://link.aps.org/doi/10.1103/PhysRevA.45.600>.
- [22] Goda, K. & Jalali, B. Dispersive fourier transformation for fast continuous single-shot measurements. *Nature Photonics* **7**, 102 (2013).
- [23] Han, Y. & Jalali, B. Photonic time-stretched analog-to-digital converter: Fundamental concepts and practical considerations. *J. Lightwave Technology* **21**, 3085 (2003).
- [24] Wong, J. *et al.* Photonic time-stretched analog-to-digital converter amenable to continuous-time operation based on polarization modulation with balanced detection scheme. *J. Lightwave Tech.* **29** (2011).
- [25] Cross, M. C. & Hohenberg, P. C. Pattern formation outside of equilibrium. *Rev. Mod. Phys.* **65**, 851–1112 (1993).
- [26] Venturini, M. & Warnock, R. Bursts of coherent synchrotron radiation in electron storage rings: A dynamical model. *Phys. Rev. Lett.* **89**, 224802 (2002). URL <http://link.aps.org/doi/10.1103/PhysRevLett.89.224802>.
- [27] Roussel, E., Evain, C., Szwaj, C. & Bielawski, S. Microbunching instability in storage rings: Link between phase-space structure and terahertz coherent synchrotron radiation radio-frequency spectra. *Phys. Rev. ST Accel. Beams* **17**, 010701 (2014).
- [28] Bai, M. *et al.* Stochastic beam dynamics in quasi-isochronous storage rings. *Phys. Rev. E* **55**, 3493–3506 (1997). URL <http://link.aps.org/doi/10.1103/PhysRevE.55.3493>.
- [29] Chao, A. W. (ed.) *Physics of collective beam instabilities in high energy accelerators* (Wiley, New York, 1993).
- [30] Krupin, O. *et al.* Temporal cross-correlation of x-ray free electron and optical lasers using soft x-ray pulse induced transient reflectivity. *Optics Express* **20**, 11396 (2012).
- [31] Riedel, R. *et al.* Single-shot pulse duration monitor for extreme ultraviolet and x-ray free-electron lasers. *Nature Communications* **4**, 1731 (2013).
- [32] Roy, P., Rouzières, M., Qi, Z. & Chubar, O. The ailes infrared beamline on the third generation synchrotron radiation facility soleil. *Infrared Physics and Technology* **49**, 139 (2006).